

MIT Open Access Articles

SOI-Supported Microdevice for Hydrogen Purification Using Palladium–Silver Membranes

The MIT Faculty has made this article openly available. **Please share** how this access benefits you. Your story matters.

Citation: Deshpande, Kishori et al. "SOI-Supported Microdevice for Hydrogen Purification Using Palladium–Silver Membranes." *Journal of Microelectromechanical Systems* 19.2 (2010): 402–409. Web. 5 Apr. 2012. © 2010 Institute of Electrical and Electronics Engineers

As Published: <http://dx.doi.org/10.1109/jmems.2010.2041529>

Publisher: Institute of Electrical and Electronics Engineers (IEEE)

Persistent URL: <http://hdl.handle.net/1721.1/69953>

Version: Final published version: final published article, as it appeared in a journal, conference proceedings, or other formally published context

Terms of Use: Article is made available in accordance with the publisher's policy and may be subject to US copyright law. Please refer to the publisher's site for terms of use.



SOI-Supported Microdevice for Hydrogen Purification Using Palladium–Silver Membranes

Kishori Deshpande, Jerry H. Meldon, Martin A. Schmidt, *Fellow, IEEE*, and Klavs F. Jensen

Abstract—High-purity hydrogen continues to receive attention as a promising energy source for fuel cells in portable power applications. On-demand hydrogen generation via fuel reforming offers a convenient alternative to hydrogen storage, but the concomitant CO generation is deleterious to the fuel cell catalyst. Of the possible hydrogen purification options, palladium membranes allow a compact design suitable for portable applications. We present a micromembrane device built in silicon-on-insulator wafers for hydrogen purification. The design imparts structural stability to a submicrometer-thick palladium–silver membrane, enabling hydrogen purification at higher pressures than were tolerated by previous devices with supported thin palladium membranes. The devices are manufactured using bulk micromachining techniques including photolithography, plasma, and wet etching. They are operated at pressures up to 2 atm with a correspondingly enhanced hydrogen flux. In particular, thin (200 nm) palladium–silver membrane yield high permeation rates of up to 50 mol/m²/s at 350 °C. The different transport resistances controlling hydrogen permeation in the micromembrane system are evaluated. [2009-0202]

Index Terms—Hydrogen, micromachining, palladium alloys, silicon-on-insulator (SOI) technology.

I. INTRODUCTION

HIGH-PURITY hydrogen has many industrial applications [1], [2] and continues to receive attention as a promising energy source for fuel cells in portable power applications [3]–[5]. The challenge of achieving high-density storage of hydrogen and safety concerns have driven efforts to produce hydrogen as needed from less hazardous and more conventional fuels, specifically by onboard hydrocarbon reforming [6], [7]. However, reforming processes generate trace amounts of carbon monoxide that must be removed from the hydrogen stream to avoid possible poisoning of the fuel cell [8]. The formed carbon monoxide can be removed by water-gas-shift, methanation, and/or selective oxidation [7], but at the expense of increasing system volume and complexity.

Palladium-based micromembrane reactors are a promising alternative approach to hydrogen purification [9]–[13]. At ele-

vated temperatures (> 250 °C), palladium films (or in practice palladium–silver alloy films for improved mechanical properties [14]) allow rapid pressure-driven permeation of hydrogen; and as they are impervious to other gases, they yield high-purity hydrogen. Tong *et al.* [13] cosputtered 1- μ m-thick palladium–silver alloy films on $\langle 110 \rangle$ -oriented silicon wafer and reported hydrogen permeation rates of up to 0.5 mol/m²/s. The films exhibited mechanical strength up to 5-atm transmembrane pressure at room temperature. Similarly, Zhang *et al.* [12] reported hydrogen fluxes of up to 0.8 mol/m²/s in 2.5- μ m palladium membranes sputtered on a 50- μ m-thick structured nickel support. Wilhite *et al.* [13] used thin (200 nm) palladium–silver films supported on perforated silicon oxide-nitride support layers to achieve hydrogen permeation rates of up to 35 mol/m²/s. The authors attributed the high fluxes to the 200-nm-thick supported membrane architecture. However, the thin membrane structure limited operation to subatmospheric transmembrane pressures.

There is an extensive literature on high-pressure operation with membranes thicker than 1 μ m [15]–[18]. However, deploying thicker membranes requires investment in expensive palladium metal, which is compounded by the larger membrane areas necessitated by lower fluxes. Thin membranes with robust structural support combine the advantages of high permeation and necessary structural stability for operation at elevated pressures. Here, we describe such a microdevice that combines robust silicon membrane support with thin palladium–silver membranes (200 nm), enabling hydrogen purification at higher pressures than were possible in earlier devices [9].

II. DESIGN CONCEPT AND STRUCTURE

The use of thin membranes at high feed pressures is motivated by gas permeation rates varying inversely with membrane thickness and increasing with transmembrane pressure. However, the maximum allowable pressure, i.e., the burst pressure of the membrane, decreases with thickness. Consequently, in principle, there is an optimum thickness that maximizes the practically attainable permeation rates. In the design reported by Wilhite *et al.* [9], 200-nm palladium–silver films were supported on a 500-nm silicon nitride-oxide support. A patterned array of 4- μ m diameter holes in the support allowed gas access to the active palladium membrane [Fig. 1(a)] Although these films exhibited excellent hydrogen permeation, the transmembrane pressure was limited to ~ 0.7 atm by the mechanical properties of the support structure.

An attractive solution for a robust support is to fabricate the reactor using silicon-on-insulator (SOI) wafer [Fig. 1(b)]. The

Manuscript received August 18, 2009; revised November 30, 2009. First published March 17, 2010; current version published April 2, 2010. Subject Editor R. Ghodssi.

K. Deshpande is with Dow Chemical Company, Freeport, TX 77541 USA.

J. H. Meldon is with the Department of Chemical and Biological Engineering, Tufts University Medford, MA 02155 USA.

M. A. Schmidt is with the Microsystems Technology Laboratories, Electrical Engineering and Computer Science, Massachusetts Institute of Technology, Cambridge, MA 02139 USA.

K. F. Jensen is with the Department of Chemical Engineering and the Department of Electrical Engineering and Computer Science, Massachusetts Institute of Technology, Cambridge, MA 02139 USA (e-mail: kfjensen@mit.edu).

Color versions of one or more of the figures in this paper are available online at <http://ieeexplore.ieee.org>.

Digital Object Identifier 10.1109/JMEMS.2010.2041529

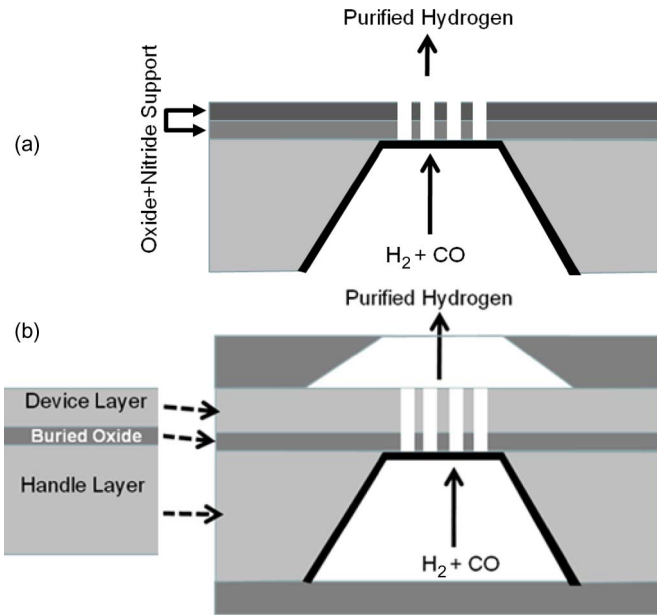


Fig. 1. Cross-sectional schematics of (a) silicon nitride-oxide-supported palladium-silver membrane (heavy black line) [9]. (b) SOI-supported palladium-silver membrane device.

palladium-silver films in this design are deposited on the buried oxide and thus become supported by buried oxide and device layer silicon [Fig. 1(b)]. This construction leads to a stronger support, allowing operation at higher pressure even with thin (200 nm) palladium membranes.

To analyze the feasibility for elevated pressure hydrogen purification, mechanical design calculations were performed. First, the maximum pressure tolerated by the silicon device layer was computed on the basis of the stress generated within the device layer as a function of buried oxide thickness, palladium-silver film thickness and hole diameter. Even with a device layer silicon thickness of only 15 μm the theoretical maximum operating pressure exceeded 8 atm. Wafers with a device layer thickness of 50 μm were used in this paper. Next, the stress in the membrane at a given pressure was compared to the tensile strength of palladium-silver (180 MPa, [13]). Treating the membrane as a fixed supported circular disk of uniform thickness (δ), the internal stress, σ , was estimated as follows:

$$\sigma = 6M_c/\delta^2 \dots, \quad \text{with } M_c = P d^2(1 + \nu)/16 \dots \quad (1)$$

Here, M_c is the bending moment along the center, P is the applied pressure, d is the hole diameter, and ν is the Poisson ratio [19]. For a given device layer thickness, the maximum allowable operating pressure depends on the burst pressure of the palladium-silver film. With a 12 μm hole diameter, the burst pressure of a 200-nm-thick palladium film is ~ 2 atm (Fig. 2).

Based on these results and the etching capabilities of the deep reactive ion etch (DRIE), the hole diameter was set at 8 μm . Calculations were also carried out to estimate reactor dimensions and pressure drops under anticipated operating conditions. The optimum channel dimensions were determined to be 15 mm long, 1.5 mm wide, and 600 μm deep.

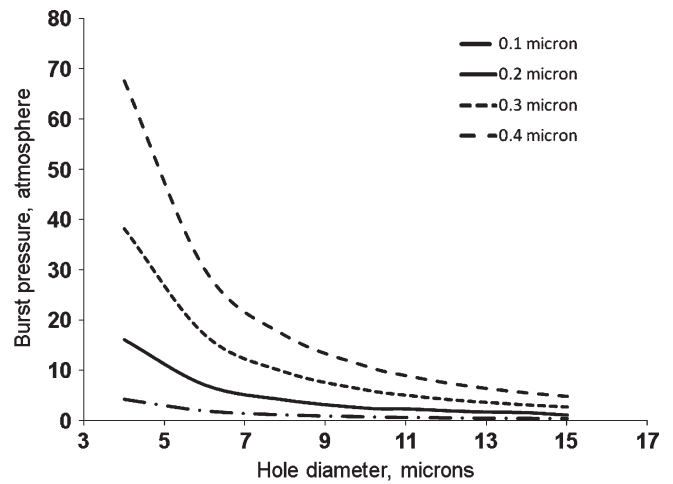


Fig. 2. Burst pressure of palladium-silver film as a function of supporting membrane hole diameter for different film thicknesses.

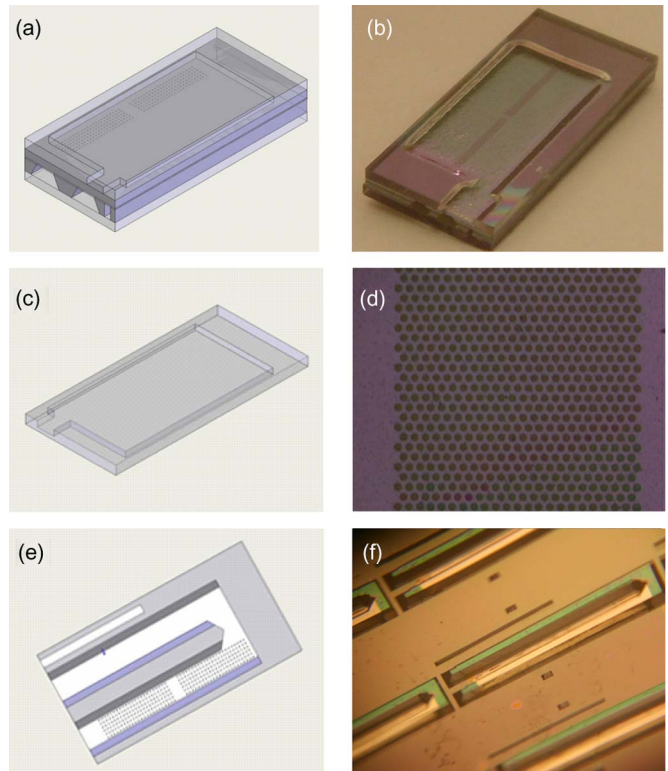


Fig. 3. Images of hydrogen purification microdevice and its major components. (a) Rendering of the devices showing the top and bottom Pyrex layers and the middle SOI layer with array of holes. (b) Photograph of fabricated device. (c) Drawing of top Pyrex layer viewed from the channel side. (d) Front side of SOI device layer with DRIE defined holes for flow of hydrogen permeating through the underlying palladium-silver membrane. (e) Three-dimensional rendering of handle layer with its KOH-etched channels as viewed from the channel side. (f) Photograph of back side of processed silicon wafer showing the palladium-silver film in the lower right hand portion of the U-shaped channel.

The final design is shown in Fig. 3(a) along with details of its major components. The device consists of three layers formed in a SOI wafer anodically bonded on both sides to Pyrex layers. A sweep channel is etched 500 μm deep and 6 mm wide in the top Pyrex layer to allow the permeated hydrogen to be swept out of the device by an inert gas such as nitrogen. This top Pyrex layer [Fig. 3(c)] is bonded to the device layer of the

SOI wafer into which an array of 8- μm diameter holes DRIE is etched [Fig. 3(d)]. These holes enable the hydrogen permeating through the palladium membrane to reach the sweep gas channel in the top Pyrex layer. The U-shaped feed gas channel underneath the palladium–silver membrane [Fig. 3(e) and (f)] is KOH-etched in the handle layer 1.3 mm wide (at the silicon surface) and 600 μm deep. The channel is closed by an anodically bonded Pyrex layer. Only the left-hand side of the U contains a palladium–silver membrane [Fig. 3(f)]. The right-hand side is included in the design to enable future inclusion of catalyst to heat the device by burning residual hydrogen as well as fuels originating from a reforming device. Here, we only discuss the hydrogen purification application and the device. Details of device fabrication are given in the next section.

III. EXPERIMENTAL PROCEDURES

A. Fabrication

The fabrication involved three 6-in wafers. Top and bottom Pyrex wafers were 2 and 0.65 mm thick, respectively. The middle wafer was a 650- μm -thick SOI wafer with 50- μm device layer thickness, 600- μm handle layer, and 1- μm buried oxide. Processing of the top and middle wafers is described separately. Forty-four devices were processed per wafer stack.

B. SOI (Middle) Wafer

The processing began with the thermal growth of a 0.25- μm -thick oxide layer [Fig. 4(b)] that protected the device layer silicon during the subsequent KOH etching steps. The thermal oxide growth was followed by low-pressure chemical vapor deposition (LPCVD) of a 0.3- μm low-stress silicon nitride layer, which served as a masking layer during KOH etch of the handle-side silicon. Eight-micrometer diameter holes on 8 μm centers were patterned on the device layer side of the SOI wafer using contact lithography and AZP 9620 thick resist [Fig. 4(c)]. In the patterned holes, nitride was etched using dry SF_6 (LAM 490B) and the oxide was removed by wet etching with a buffered oxide solution of HF and NH_4F . Next, the holes were formed in device layer silicon by DRIE (STS Multiplex ICP) [Fig. 4(d)]. Etch and passivation cycle times were manipulated to ensure uniform etch across the wafer and vertical side walls. In order to prevent footing of the buried oxide layer, etching was monitored using an interferometer. The resist was then removed using piranha (3 : 1 sulfuric acid: hydrogen peroxide) and an oxygen plasma removed residual polymeric deposits formed during the DRIE passivation cycle. In the next step [Fig. 4(e)], a 0.5- μm -thick silicon oxide was thermally grown on the RCA cleaned wafer at 1000 $^\circ\text{C}$ to protect the silicon during the subsequent KOH etching.

The feed gas channels were defined in the handle layer by standard photolithography and thick resist (AZP 9620). The exposed nitride and oxide were then etched using SF_6 and buffered oxide etch (BOE, 6:1 volume ratio of 40% NH_4F in water to 49% HF in water) while protecting the front side with photoresist [Fig. 4(f)]. Next, the handle layer silicon was etched with 20% KOH solution at 80 $^\circ\text{C}$ using a Teflon chuck to protect the front side [Fig. 4(g)]. The observed etch rate was 80 μm of

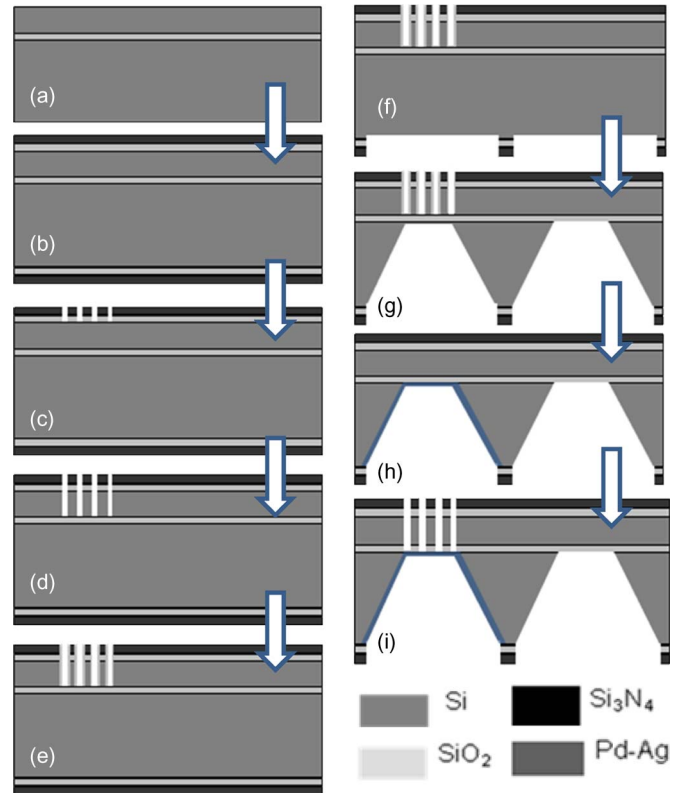


Fig. 4. Fabrication of the middle device layer. (a) 0.25- μm thermally grown oxide layer (b) LPCVD of 0.3- μm low-stress silicon nitride layer. (c) Patterned 8- μm diameter holes on the front side of the device layer and etched into the silicon nitride and oxide layers. (d) Holes etched in device layer silicon by DRIE and resist removed. (e) Growth of 0.5 μm thick thermal oxide. (f) Definition of feed gas channels in the handle layer and removal of exposed nitride and oxide layers. (g) KOH etching of handle layer silicon layer using a Teflon chuck to protect the front side. (h) E-beam deposition of palladium–silver film. (i) Removal of buried oxide on top of the palladium–silver membrane.

silicon per hour. Upon successful KOH etch, the device was ready for palladium–silver film deposition. A 10-nm titanium layer was electron beam deposited at 10^{-6} torr to promote adhesion of the palladium film. This titanium deposition was followed by alternate deposition of palladium (29.8 nm) and silver (12.9 nm) to yield a film thickness of 200 nm and silver content of 23 wt.% [Fig. 4(h)]. Finally, the top of the palladium–silver membrane was released by etching the buried oxide using BOE [Fig. 4(i)]. The thermally grown oxide (step e) helped wet the walls of the otherwise hydrophobic silicon hole making feasible etching of the 50- μm -deep seated oxide layer. The wafer was cleaned with acetone, methanol, and isopropyl alcohol and dried at 120 $^\circ\text{C}$ in a convection oven.

C. Top Wafer

Fluidic channels on the top Pyrex glass (Bullen Ultrasonics, 2 mm thick) were etched using a 49% hydrofluoric acid etch process. Processing began with electron beam deposition of a chrome-gold mask on both sides of a piranha-cleaned wafer. Fifty-nanometer chrome was deposited to promote adhesion of a 200-nm gold layer to Pyrex. The fluidic channels were transferred to the metalized Pyrex wafer using contact lithography and thick photoresist (AZ 5690—10 μs). The gold layer was then removed with a gold etchant (Gold Etch TFA,

Transene Inc. Danvers, MA) followed by a chrome etch (CR-7 Chrome Etch, Cyantek CA). Glass was etched using 49% hydrofluoric acid. While most workers use this technique for etch depths up to 500 μm by first annealing the gold-chrome layer [20], [21], we obtained 500- μm -deep trenches without wafer annealing. The gold-chrome mask remained intact during the etch, which resulted in well-defined channels. Finally, the resist was stripped using piranha solution followed by gold and chrome layer removal. Since hydrofluoric acid is an isotropic etch, channel dimensions were optimized using a master mask with channels of varying dimensions to develop a calibration curve.

D. Final Processing

The back side of the middle device wafer was anodically bonded (EV 450) with a Pyrex wafer to form the feed channels. Bonding for 10 min of 900 V at 350 $^{\circ}\text{C}$ was sufficient to form a leak-free bond. The two-wafer stack was then flipped and the processed Pyrex wafer aligned on the front side of the silicon wafer to enclose the array of holes from the membrane area within the sweep channels in Pyrex. Using the conditions previously mentioned, the wafers were bonded to form the final device. Finally, the three wafer assembly was cut into individual devices using a die saw (Disco Abrasive System Model DAD-2H/6T). Forty-four devices were obtained from each wafer. A $\sim 100\%$ yield of fabricated devices was achieved, but the actual number of functional devices was typically slightly lower because of occasional defects in the palladium–silver membranes.

E. Packaging

Stainless steel capillaries, with outer diameter 450 μm and inner diameter 350 μm , were used to make fluidic connections. Stainless steel was preferred over glass capillaries owing to its fracture toughness. Identifying a sealant suitable at the operating temperature was critical. While common epoxy suffices up to 250 $^{\circ}\text{C}$, high-temperature brazes must be heated to above 500 $^{\circ}\text{C}$ to ensure a good seal. Importantly, palladium–silver membranes begin to agglomerate at 500 $^{\circ}\text{C}$, which imposes an upper temperature limit for brazing. Different compositions were tested for a leak proof seal. Epoxy (Epotek) was satisfactory up to 300 $^{\circ}\text{C}$, but did withstand pressures above 1 atm. Glass braze from SEM COM, (Toledo Ohio) with a thermal expansion coefficient comparable to that of silicon was found to be an effective sealant at up to 475 $^{\circ}\text{C}$ and 4 atm. However, it was observed [Fig. 5(a)] that brazing in air at 475 $^{\circ}\text{C}$ could lead to membrane oxidation and subsequent agglomeration during device testing. Furthermore, brazing at pressures as low as 70 mtorr was insufficient to protect the membrane from oxidation.

In order to prevent membrane oxidation at high temperature even under vacuum, localized brazing was carried out. A handheld butane torch with a 2-mm nozzle tip and maximum temperature of 1200 $^{\circ}\text{C}$ was used to heat the device in air. Silicon's high thermal conductivity ensured that the device temperature did not exceed 400 $^{\circ}\text{C}$ even while maintaining the braze temperature of 600 $^{\circ}\text{C}$. Furthermore, the high temperature annealed

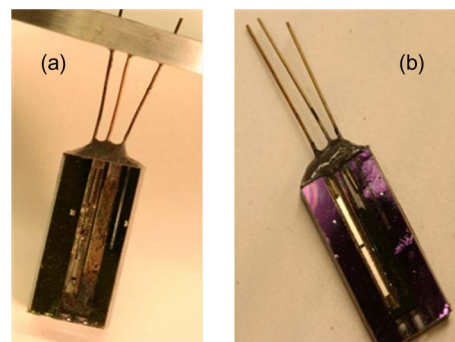


Fig. 5. Effect of brazing on membrane structure. (a) Brazing in furnace in air at 475 $^{\circ}\text{C}$ leads to failure of the palladium–silver membrane by agglomeration. (b) Five-minute brazing preserves the membrane.

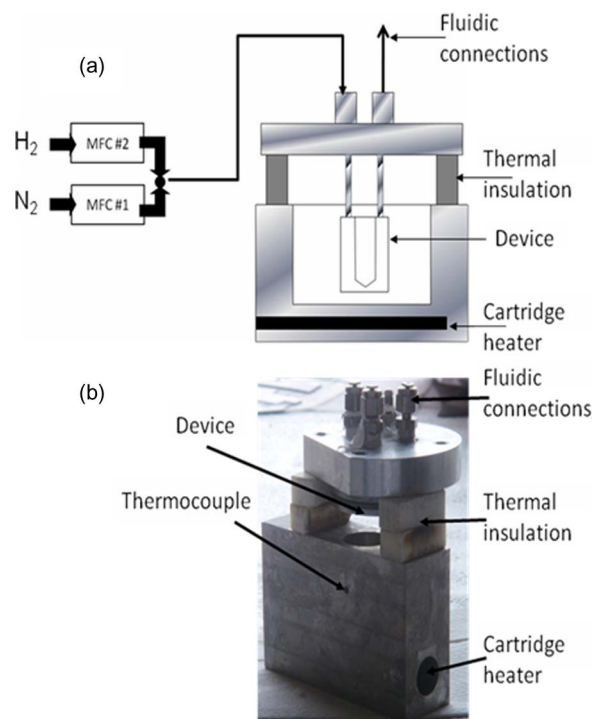


Fig. 6. Experimental setup for testing the hydrogen purification devices. (a) Schematic. (b) Photograph.

the stainless steel capillaries, making them more ductile and easy to place in the testing jig. Finally, to relieve the thermal stresses generated in the glass during rapid brazing, the braze was annealed from 475 $^{\circ}\text{C}$ to 450 $^{\circ}\text{C}$ at 1.5 $^{\circ}\text{C}$ per minute. Using this approach, multiple devices could be sealed in half an hour without damaging the palladium–silver film, unlike controlled heating in a furnace for 12 h, which resulted in palladium–silver agglomeration.

F. Experimental Setup

The experimental setup (Fig. 6) consisted of an aluminum chuck with built-in cartridge heaters. The device was mounted on an aluminum plate with holes aligned to the capillaries using a quick-drying epoxy (Devcon). The aluminum plate was then mounted on a holder fitted with standard Swagelok connections for feed gases. The assembly was then placed in the

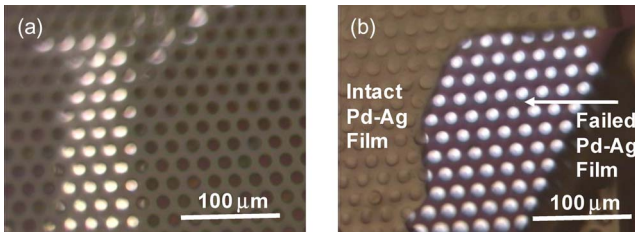


Fig. 7. (a) Image of the top of the supporting holes in silicon. (b) Image from the bottom showing a section of a still intact membrane and a peeled section.

aluminum chuck for high-temperature experiments. Temperature was monitored using a type K thermocouple (Omega) fitted in the aluminum chuck. A mixture of hydrogen and nitrogen was fed to the feed side using a mass flow controller (UFC-1100 model, UNIT) allowing a wide range of compositions. Helium was fed to the sweep side via another mass flow controller. The exiting sweep gas was analyzed using an Inficon ICP400 mass spectrometer. From this information the sweep side hydrogen composition and membrane selectivity were estimated. All gases were grade 5 purity (> 99.999%) supplied by BOC gases.

The packaged and brazed device was leak tested and the integrity of the membrane evaluated before characterizing hydrogen separation. Postfabrication membrane integrity was checked by feeding a mixture of hydrogen and nitrogen at 10 sccm and 1 atm. Helium was employed as a sweep gas and the permeate gas composition measured using the mass spectrometer. In the event of a defect in the membrane, such as a pinhole, nitrogen would pass through the membrane and be detected by the mass spectrometer. To check the maximum allowable feed pressure, hydrogen was fed at increasing pressure at 350 °C and the permeate composition checked using a constant helium flow rate of 100 sccm. A membrane failure showed up as a sudden increase in hydrogen content.

IV. RESULTS AND DISCUSSION

The new SOI design enabled operation of the 200-nm-thick membrane at 350 °C up to a burst pressure of 2 atm, which is considerably lower than the predicted failure pressure of 4 atm (Fig. 2). Inspection of the top and bottom hole diameters of the failed membrane using back light (Fig. 7) revealed that the palladium–silver membrane had not burst at individual holes, but instead had peeled off. Furthermore, the actual diameter of the holes at the top of the wafer was 10.5 μm while the diameter at the bottom (the side in contact with the palladium–silver membrane) was ≈ 13 μm. This enlargement in hole dimension could have occurred during the photolithography, deep reactive ion etching (step d, Fig. 4) and/or BOE (step i, Fig. 4) steps. The burst pressure of a 13 μm diameter hole is about 1.9 atm, and so it is possible that the film fractured at a few locations, and internal stresses in the film then caused it to peel away from the underlying silicon support.

Permeation rates were measured at 350 °C with feed hydrogen partial pressures ranging from 0.1 to ~2 atm (Fig. 8). Hydrogen fluxes in the lower pressure regime compare well with those measured previously in our laboratory in membranes of the same 200-nm thickness, but supported on silicon nitride

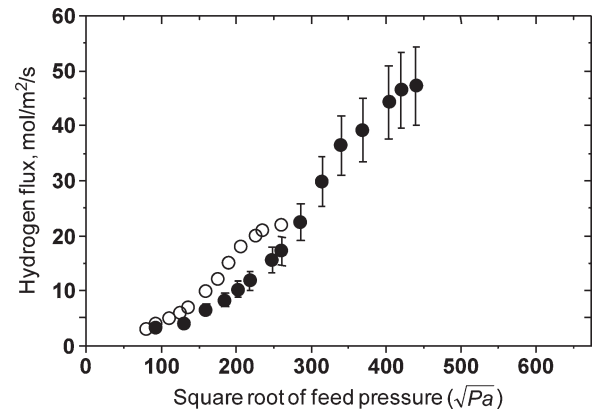


Fig. 8. Hydrogen permeation as a function of square root of feed H_2 partial pressure ●: current work, ○: Wilhite *et al.* [9].

membranes [9]. The H_2 to N_2 selectivity was determined to be greater than 1000—also in agreement with previous studies on these thin Pd–Ag membranes. The alternating deposition of Pd and Ag films and subsequent anneal could have the beneficial effect of increasing film ductility and decreasing pin holes.

Table I compares measured fluxes obtained in this paper with literature data. Permeation of hydrogen through palladium depends directly on temperature, pressure and inversely with membrane thickness. Hence, the higher permeation observed in this paper could be due to higher applied pressure, thinness of the membrane and/or operating temperature. The difference in the observations for the cited literature is explained in the following paragraphs.

Karnik *et al.* [22] reported permeation data at 100 °C and ~0.5 atm, whereas the permeation data in this paper were obtained at 350 °C and as a function of increasing feed pressure. Thus, the higher flux in our case could be explained by higher temperature as well as feed pressure. Orders of magnitude lower fluxes reported by Ye *et al.* [23] for Pd membranes indicate permeation control by phenomena other than diffusion of H atoms in bulk metal. They also reported H_2/He selectivity of only 10 and very low H_2 fluxes that increased with increasing temperature. Tong *et al.* [13] report more robust 1-μm-thick membranes that can withstand 4-atm pressure. Although their membranes withstood high pressure, permeation experiments were run with 1 atm on both sides and hydrogen partial pressure differences in the range 0–0.3 atm.

The experimental data reported here (Fig. 8, darkened circles) exhibit regimes of upward and downward concavity. The lower H_2 partial pressure (P_{H_2}) data, obtained feeding H_2/N_2 mixtures (8–99 mol% H_2) at 1 atm, is concave upward. The higher pressure data, obtained feeding pure hydrogen at between 1 and 2 atm, is concave downward. In all experiments, helium sweep gas diluted permeating hydrogen to maintain the permeation driving force. Quantitative interpretation of the data is complicated by several factors.

Because much of the hydrogen in the feed gas permeated, P_{H_2} values in the sweep gas and, with mixed gas feeds, in the feed gas as well, changed significantly along the flow channels. Thus, there were large decreases along the membrane in the difference between feed and sweep gas P_{H_2} values and

TABLE I
COMPARISONS OF Pd MEMBRANE HYDROGEN MICRODEVICE PURIFICATION STUDIES

	Membrane Material	Thickness (μm)	Temp ($^{\circ}\text{C}$) H_2 Pres (atm)	Membrane support	Flux ($\text{mol}/\text{m}^2\text{-s}$)	Channel depth (μm)
Present study	$\text{Pd}_{0.77}\text{Ag}_{0.23}$	0.2	350 < 2	Silicon with etched holes	46	600
Karnik <i>et al.</i> [22]	Pd	0.2	100 ~ 0.5	Spin on glass	5	Not available
Zhang <i>et al.</i> [12]	Pd	2.5	200-400 ~ 0.2	50 μm Nickel	0.8	65
Wilhite <i>et al.</i> [9]	$\text{Pd}_{0.77}\text{Ag}_{0.23}$	0.2	350 < 1	Silicon nitride	22	600
Keurentjes <i>et al.</i> [11]	Pd-Ag	1	400-500 < 1	Silicon nitride	1	~ 350
Ye <i>et al.</i> [23]	Pd	0.34	250 ~ 2	30 μm porous silicon	0.112	~ 300
Tong <i>et al.</i> [13]	$\text{Pd}_{0.77}\text{Ag}_{0.23}$	1	450 < 1	Silicon oxide	0.5	~ 350

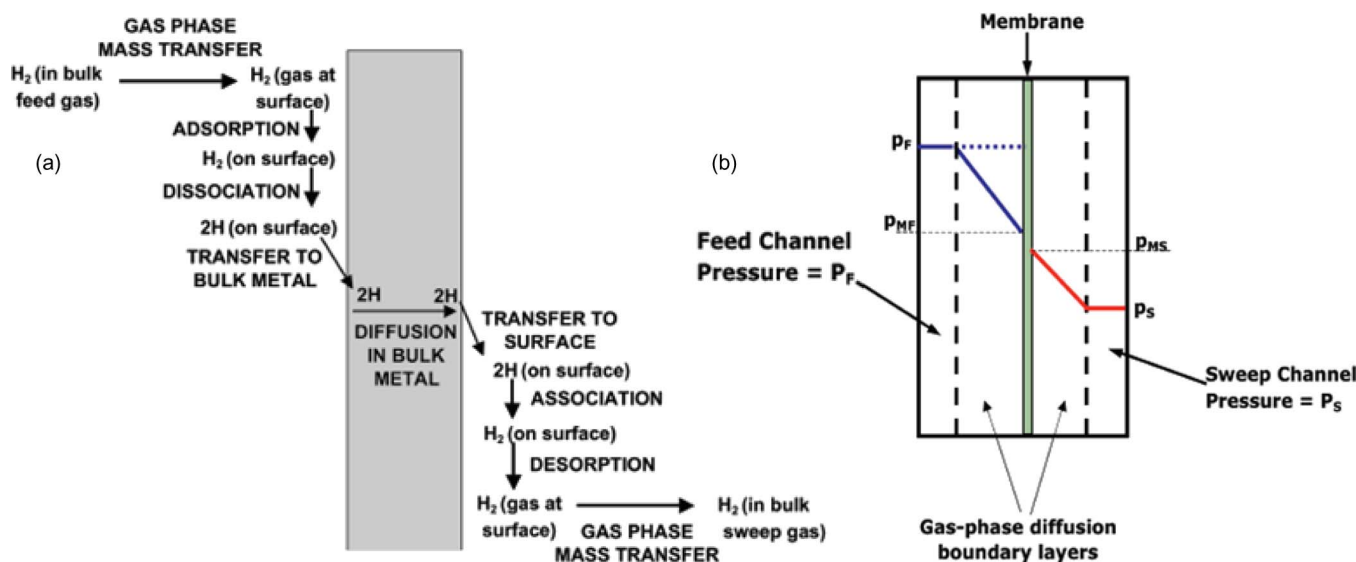


Fig. 9. (a) Schematic of the sequence of steps in the overall hydrogen permeation process, each of which, in principle, may be a rate limiting step. (b) Schematic illustration of partial pressure profiles when gas-phase diffusion limits permeation.

corresponding decreases in what is generally considered the permeation driving force (as explained hereinafter): the difference between $\sqrt{p_{\text{H}_2, \text{feed}}}$ and $\sqrt{p_{\text{H}_2, \text{sweep}}}$. In the experiments with mixed feeds, 15%–40% of the hydrogen permeated, as a result of which $p_{\text{H}_2, \text{feed}}$ decreased by an average of 15%, while the helium sweep gas exited with as much as 19% (by volume) hydrogen. Consequently, the transmembrane p_{H_2} difference, Δp_{H_2} , decreased between entrance and exit by $\approx 20\%$, except with the lowest $p_{\text{H}_2, \text{feed}}$, when it decreased by 40%.

In Fig. 8, fluxes are plotted versus $\sqrt{p_{\text{H}_2, \text{feed}}}$ (rather than Δp_{H_2}) because, as discussed hereinafter, equilibrium hydrogen concentrations in metallic membranes are proportional to $\sqrt{p_{\text{H}_2}}$. Accordingly, permeation rates in sufficiently thick membranes are proportional to $\Delta\sqrt{p_{\text{H}_2}}$, and $\Delta\sqrt{p_{\text{H}_2}} \approx \sqrt{p_{\text{H}_2, \text{feed}}}$ only when $\sqrt{p_{\text{H}_2, \text{sweep}}} \approx 0$. In our experiments, as just previously noted, $\sqrt{p_{\text{H}_2, \text{sweep}}}$ values were substantial; consequently, $\sqrt{p_{\text{H}_2, \text{feed}}}$ values do not accurately represent the $\Delta\sqrt{p_{\text{H}_2}}$ values. As such, it would have been more appropriate to plot flux versus $\Delta\sqrt{p_{\text{H}_2}}$, if not for the fact that the high permeation rates

caused $\Delta\sqrt{p_{\text{H}_2}}$ to decrease along the membrane by up to 70%. Thus, choosing $\Delta\sqrt{p_{\text{H}_2}}$ values for such a plot would have been somewhat arbitrary.

Aside from the marked decrease in $\Delta\sqrt{p_{\text{H}_2}}$ values along the membrane, quantitative interpretation of the data is also made difficult by gas-phase diffusion that, according to our analysis as described hereinafter, substantially limited hydrogen permeation rates. Fig. 9 shows the complex sequence of steps in the overall hydrogen permeation process, each of which, in principle, may constitute a bottleneck. The surface phenomena—adsorption, dissociation, dissolution in bulk metal at the high p_{H_2} surface, and the reverse processes at the low p_{H_2} surface—are generally assumed to be instantaneous within the time frame of hydrogen diffusion in bulk metal. However, this assumption breaks down when the surface is sufficiently “poisoned” (adsorption sites are occupied by competing gases), the membrane is so thin or the temperature so low that the time scale of bulk diffusion is comparable to or less than that of at least one of the surface processes [24].

When bulk diffusion *does* control permeation and dissolved hydrogen concentrations are low, the hydrogen flux (J_M) varies with the values of p_{H_2} and membrane thickness L_M as follows:

$$J_M = \frac{K_M (\sqrt{p_{H_2,feed}} - \sqrt{p_{H_2,sweep}})}{L_M} \quad (2)$$

and K_M , the membrane permeability, varies according to

$$K_M = A e^{-\frac{B}{T}} \quad (3)$$

where T is the absolute temperature, and A and B are constants for a given Pd alloy; K_M for Pd/Ag (23 wt.% silver) at 350 °C is $\approx 4 \times 10^{-6}$ mol-m/(m²-s-atm^{0.5}) [25].

Strictly speaking, the p_{H_2} values in (2) are the partial pressures at the respective feed and sweep-side membrane *surfaces* [which are denoted by p_{MF} and p_{MS} in Fig. 9(b)]. When the feed gas is pure hydrogen, or when the feed and sweep gases are mixed to the extent that p_{H_2} is independent of distance from the membrane surface (although it may vary *along* that surface), the partial pressures in the *bulk* gases (which are denoted in Fig. 9(b) by p_F and p_S) may be inserted in (2).

In general, however, $p_{MF} \neq p_F$ and $p_{MS} \neq p_S$ because of the gas-phase boundary layers that generally prevail at solid/fluid interfaces, in which there is negligible lateral mixing. Hydrogen transfer across these boundary layers is via molecular diffusion driven by partial pressure differences, i.e., $(p_F - p_{MF})$ and $(p_{MS} - p_S)$. Under the laminar experimental flow conditions, the boundary layer thicknesses were roughly half the channel heights (h), and approximate values for the boundary layer hydrogen fluxes (J_{BL}) may be estimated as follows [26]:

$$J_{BL,F} \approx \frac{2D_{H_2/N_2}}{h_F RT} (p_F - p_{MF}) \quad (4)$$

$$J_{BL,S} \approx \frac{2D_{H_2/He}}{h_S RT} (p_{MS} - p_S) \quad (5)$$

where the binary diffusion coefficients D_{H_2/N_2} and $D_{H_2/He}$ at 350 °C are $\approx 3 \times 10^{-4}$ and 5×10^{-4} m²/s, respectively; gas constant $R = 8.21 \times 10^{-5}$ m³-atm/(mol-°K); h_F and h_S are approximately 6×10^{-4} m each; and ideal-gas behavior has been assumed in light of the temperature and relatively low pressures.

The theoretical calculations of Ward and Dao [24] suggest that at 350 °C, hydrogen permeation in unalloyed palladium membranes is bulk diffusion-controlled even when L_M is only 0.2 μ m. Assuming the same to be true of the 0.2 μ m Pd/Ag (23 wt.% silver) membrane tested in this paper, (2) may be rewritten as:

$$J_M = \frac{K_M (\sqrt{p_{MF}} - \sqrt{p_{MS}})}{L_M} = \frac{K_M (p_{MF} - p_{MS})}{L_M (\sqrt{p_{MF}} + \sqrt{p_{MS}})} \quad (6)$$

Equating the J expressions in (4)–(6) yields the following expression for the theoretical steady-state hydrogen flux:

$$J = \frac{p_F - p_S}{r_F + r_M + r_S} \quad (7)$$

where the *mass transfer resistances* r are defined as follows:

$$r_M \equiv \frac{L_M (\sqrt{p_{MF}} + \sqrt{p_{MS}})}{K_M} \quad (8)$$

$$r_F \equiv \frac{RTh_F}{2D_{H_2/N_2}} \quad (9)$$

$$r_S \equiv \frac{RTh_S}{2D_{H_2/He}} \quad (10)$$

Taking 1.0 atm^{0.5} as a nominal value for $\sqrt{p_{MF}} + \sqrt{p_{MS}}$, the estimated r_M , r_F and r_S values are, respectively, 0.05, 0.05 and 0.03 atm-m²-s/mol. Taking 1 atm as a nominal value for $p_F - p_S$, the estimated flux J is 8 mol/(m²-s), which compares well with the experimental fluxes of 3–30 mol/(m²-s) that were measured with mixed feed gases. Apparently, gas-phase mass transfer resistances were quite significant. Had they been absent, the hydrogen fluxes would likely have been double those recorded.

V. CONCLUSION

The new micromembrane device for hydrogen purification was built in SOI wafers to provide structural stability to a submicrometer-thick palladium–silver membrane. This design modification made hydrogen purification possible at higher pressures than in previous devices with supported thin palladium membranes. Specifically, the devices were operated at pressures up to 2 atm with a correspondingly enhanced hydrogen flux. Thin (200 nm) palladium–silver membrane yield high permeation rates of up to 50 mol/m²/s at 350 °C. An analysis of the transport resistances controlling hydrogen permeation in the micromembrane system suggested that the process was limited by gas-phase diffusion and that even larger fluxes would be possible with improved flow channel designs. The large fluxes observed with the present design and the potential for further improvements show promise as high-pressure hydrogen purification units for portable applications.

REFERENCES

- [1] R. Ramachandran and R. K. Menon, "An overview of industrial uses of hydrogen," *Int. J. Hydrogen Energy*, vol. 23, no. 7, pp. 593–598, Jul. 1998.
- [2] F. Dimeo, I. S. Chen, P. Chen, J. Neuner, A. Roerhl, and J. Welch, "MEMS-based hydrogen gas sensors," *Sens. Actuators B, Chem.*, vol. 117, no. 1, pp. 10–16, Sep. 2006.
- [3] National Research Council, *Meeting the Energy Needs of Future Warriors*. Washington, DC: Nat. Academies Press, 2004.
- [4] C. K. Dyer, "Replacing the battery in portable electronics," *Sci. Amer.*, vol. 281, pp. 88–93, Jul. 1999.
- [5] L. Schlapbach and A. Zuttel, "Hydrogen-storage materials for mobile applications," *Nature*, vol. 414, no. 6861, pp. 353–358, Nov. 2001.
- [6] L. R. Arana, S. B. Schaevitz, A. J. Franz, M. A. Schmidt, and K. F. Jensen, "A microfabricated suspended-tube chemical reactor for thermally efficient fuel processing," *J. Microelectromech. Syst.*, vol. 12, no. 5, pp. 600–612, Oct. 2003.
- [7] J. D. Holladay, E. O. Jones, R. A. Dagle, G. G. Xia, C. Cao, and Y. Wang, "High efficiency and low carbon monoxide micro-scale methanol processors," *J. Power Sources*, vol. 131, no. 1/2, pp. 69–72, May 2004.
- [8] Z. G. Qi, C. Z. He, and A. Kaufman, "Effect of CO in the anode fuel on the performance of PEM fuel cell cathode," *J. Power Sources*, vol. 111, no. 2, pp. 239–247, Sep. 2002.
- [9] B. A. Wilhite, M. A. Schmidt, and K. F. Jensen, "Palladium-based micromembranes for hydrogen separation: Device performance and chemical stability," *Ind. Eng. Chem. Res.*, vol. 43, no. 22, pp. 7083–7091, Oct. 2004.

- [10] A. Franz, K. F. Jensen, and M. A. Schmidt, "Palladium based micromembranes for hydrogen separation and hydrogenation/dehydrogenation reactions," in *Proc. 12th Int. Conf. Microelectromech. Syst.*, Orlando, FL, 1999, pp. 382–385.
- [11] J. T. F. Keurentjes, F. C. Gielens, H. D. Tong, C. J. M. van Rijn, and M. A. G. Vorstman, "High-flux palladium membranes based on microsystem technology," *Ind. Eng. Chem. Res.*, vol. 43, no. 16, pp. 4768–4772, Aug. 2004.
- [12] Y. Zhang, J. Gwak, Y. Murakoshi, T. Ikehara, R. Maeda, and C. Nishimura, "Hydrogen permeation characteristics of thin Pd membrane prepared by microfabrication technology," *J. Membr. Sci.*, vol. 277, no. 1/2, pp. 203–209, Jun. 2006.
- [13] H. D. Tong, J. W. E. Berenschot, M. J. D. Boer, J. G. E. Gardeniers, H. Wensink, H. V. Jansen, W. Nijdam, M. C. Elwenspoek, E. C. Gielens, and C. J. M. v. Rijn, "Microfabrication of palladium–silver alloy membranes for hydrogen separation," *J. Microelectromech. Syst.*, vol. 12, no. 5, pp. 622–629, Oct. 2003.
- [14] K. Aoki, S. Yokoyama, K. Kusakabe, and S. Morooka, "Preparation of supported palladium membrane and separation of hydrogen," *Korean J. Chem. Eng.*, vol. 13, no. 5, pp. 530–537, Sep. 1996.
- [15] K. S. Rothenberger, A. V. Cugini, B. H. Howard, R. P. Killmeyer, M. V. Ciocco, B. D. Morreale, R. M. Enick, F. Bustamante, I. P. Mardilovich, and Y. H. Ma, "High pressure hydrogen permeance of porous stainless steel coated with a thin palladium film via electroless plating," *J. Membr. Sci.*, vol. 244, no. 1/2, pp. 55–68, Nov. 2004.
- [16] R. S. Souleimanova, A. S. Mukasyan, and A. Varma, "Pd membranes formed by electroless plating with osmosis: H₂ permeation studies," *AIChE J.*, vol. 48, no. 2, pp. 262–268, Feb. 2002.
- [17] D. A. P. Tanaka, M. A. L. Tanco, S. Niwa, Y. Wakui, F. Mizukami, T. Namba, and T. M. Suzuki, "Preparation of palladium and silver alloy membrane on a porous α -alumina tube via simultaneous electroless plating," *J. Membr. Sci.*, vol. 247, no. 1/2, pp. 21–27, Feb. 2005.
- [18] S. Tosti, L. Bettinali, and V. Violante, "Rolled thin Pd and Pd–Ag membranes for hydrogen separation and production," *Int. J. Hydrogen Energy*, vol. 25, no. 4, pp. 319–325, Apr. 2000.
- [19] W. C. Young and R. G. Budynas, *Roark's Formulas for Stress and Strain*, 7th ed. New York: McGraw-Hill, 2002, p. 488.
- [20] F. E. H. Tay, C. Iliescu, J. Jing, and J. Miao, "Defect-free wet etching through pyrex glass using Cr/Au mask," *Microsyst. Technol.*, vol. 12, no. 10/11, pp. 935–939, Sep. 2006.
- [21] D. C. S. Bien, P. V. Rainey, S. J. N. Mitchell, and H. S. Gamble, "Characterization of masking materials for deep glass micromachining," *J. Micromech. Microeng.*, vol. 13, no. 4, pp. S34–S40, Jun. 2003.
- [22] S. V. Karnik, M. K. Hatalis, and M. V. Kothare, "Towards a palladium micro-membrane for the water gas shift reaction: Microfabrication approach and hydrogen purification results," *J. Microelectromech. Syst.*, vol. 12, no. 1, pp. 93–100, Feb. 2003.
- [23] S.-Y. Ye, S. Tanaka, M. Esashi, S. Hamakawa, T. Hanaoka, and F. Mizukami, "Thin palladium membrane microreactors with oxidized porous silicon support and their application," *J. Micromech. Microeng.*, vol. 15, no. 11, pp. 2011–2018, Nov. 2005.
- [24] T. L. Ward and T. Dao, "Model of hydrogen permeation behavior in palladium membranes," *J. Membr. Sci.*, vol. 153, no. 2, pp. 211–231, Feb. 1999.
- [25] E. Kikuchi and S. Uemiya, "Preparation of supported thin palladium–silver alloy membranes and their characteristics for hydrogen separation," *Gas Separ. Purif.*, vol. 5, pp. 261–266, 1991.
- [26] R. B. Bird, W. E. Stewart, and E. N. Lightfoot, *Transport Phenomena*, 2nd ed. New York: Wiley, 2002.



Kishori Deshpande received the Ph.D. degree from the University of Notre Dame, Notre Dame, IN, in 2005.

From December 2004 to April 2008, she was a Postdoctoral Researcher in Prof. Jensen's group at the Massachusetts Institute of Technology (MIT), Cambridge. She is currently a Senior Research Engineer with Dow Chemical Company, Freeport, TX. Her research at MIT focused on developing tools and techniques for realization of portable power generation using microreaction technology. Her research

interests include reaction engineering, catalysis, advanced nanomaterials and microreaction technology for chemical and biological applications.

Dr. Deshpande is a member of the American Institute of Chemical Engineers.



Jerry H. Meldon received the B.E. degree in chemical engineering from the Cooper Union, New York, NY, and the Ph.D. degree from the Massachusetts Institute of Technology (MIT), Cambridge.

He is an Associate Professor of chemical and biological engineering at Tufts University, Medford, MA. While a Postdoctoral Fellow in the Physiology Department, University of Odense, Odense, Denmark, he coauthored with Dr. Lars Garby the monograph, *The Respiratory Functions of Blood*.

Much of his recent activity has focused on postcombustion carbon dioxide capture. He is currently organizing an international workshop on that subject that is scheduled to take place in July 2010. His major research interests are in the mathematical modeling of transport processes, particularly mass transfer with simultaneous chemical reaction as a controlling factor in separation processes, reaction engineering, and reaction/separation coupling.



Martin A. Schmidt (S'88–M'85–SM'00–F'03) received the B.S. degree from the Rensselaer Polytechnic Institute, Troy, NY, in 1981, and the S.M. and Ph.D. degrees from the Massachusetts Institute of Technology (MIT), Cambridge, in 1983 and 1988, respectively.

Since 1988, he has been a Faculty Member of the Department of Electrical Engineering and Computer Science, MIT. From 1989 to 2006, he served as the Director of the Microsystems Technology Laboratories, MIT. Since 2008, he has served as Associate

Provost at MIT. His primary research interest is MEMS. He is also active in the commercialization of technology, having served as cofounder or coinventor of the core intellectual property for six start-up companies.

Dr. Schmidt is a recipient of the National Science Foundation Presidential Young Investigator Award and an Honorary Doctorate from the Technical University of Denmark. He has also received the Ruth and Joel Spira Teaching Award and the Eta Kappa Nu Teaching Award from MIT.



Klavs F. Jensen received the M.Sc. degree in chemical engineering from the Technical University of Denmark, Lyngby, Denmark and the Ph.D. degree from the University of Wisconsin, Madison.

He is the Warren K. Lewis Professor and Head of Chemical Engineering and Professor of materials science and engineering at the Massachusetts Institute of Technology, Cambridge. He serves on the Steering Committee for the International Conference on Miniaturized Systems for Chemistry and Life Sciences (μ TAS) and he Chaired the 2005 Conference in Boston, MA. His research interests revolve around microfabrication, testing, integration, and scale-up of microfluidic systems for chemical and biochemical discovery, synthesis, and processing. Chemical kinetics and transport phenomena related to processing of organic and inorganic materials for electronic and optical applications are also topics of interest along with development of simulation approaches for reactive systems.

Dr. Jensen is a member of the U.S. National Academy of Engineering and the American Academy of Arts and Sciences. He is also a Fellow of the American Association for the Advancement of Science, the American Institute of Chemical Engineers, and the Royal Society of Chemistry.